Electronic Supplementary Information

for

Iodide-assisted energy-saving hydrogen production using self-supported sulfate ion modified NiFe(oxy)hydroxide nanosheets

Shraddha Paniya, Asmita Dileep Gaonkar, Kiran Vankayala*

Functional Materials for Electrochemistry and Solar Energy (FunMatES) Group, Energy and Environmental Chemistry Lab, Department of Chemistry,
Birla Institute of Technology and Science, Pilani, K K Birla Goa Campus, Goa, 403726, India.

Contents:

1. Experimental Section:

1.1 Chemicals:

Iron (III) nitrate nonahydrate ($Fe(NO_3)_3.9H_2O$, Finar, 98%), Potassium hydroxide (KOH, Loba Chemie, 97%), Sodium thiosulphate pentahydrate ($Na_2S_2O_3.5H_2O$, Finar, 99.5%), Ethanol (C_2H_5OH, Fischer Scientific, 99.9%), Acetone (C_3H_6O, Fischer Scientific, 99%), Hydrochloric acid (HCl, Fischer Scientific), Potassium Iodide (KI, Loba Chemie, 99%), Ethylene diamine ($C_2H_4(NH_2)_2$, Loba chemie, 98%), Red phosphorus (P, Loba chemie, 98%). All chemicals were used as-received. Aqueous solutions were prepared using deionised (DI) water (Resistivity = 18.3 MΩ). Nickel foam (thickness: 1.6 mm, purity: 95%, porosity: 95%) was procured.

1.2. Preparation of self-supported oxyanion grafted NiFe (oxy)hydroxide [$(SO)_x$-NiFeOOH] on Nickel foam: Prior to the preparation of (SO_x)-NiFeOOH on Ni foam, known area of Ni foam substrates were cleaned via the following protocol: Ni foam pieces were sonicated in acetone for 10 min., followed by 10 min. sonication each in 3 M HCl, DI water and ethanol respectively. Subsequently, the dried Ni foam substrates were subjected to modification. A facile, one-step rapid method was used for the fabrication of electrodes (scheme S1) at ambient conditions.[1] Pre-cleaned Ni foam substrates of known area were immersed in a glass vial containing aqueous solutions of 0.866 mmol of $Fe(NO_3)_3.9H_2O$ and 0.316 mmol of $Na_2S_2O_3.5H_2O$ in 10 mL DI water. Here $Na_2S_2O_3.5H_2O$ acts as sulphur (S) source. After 5 min of immersion, the Ni foam was removed from the glass vial and washed thoroughly with DI water and dried at ambient temperature. A clear colour change was noticed indicating the modification of Ni foam (scheme S1) in just 5 min of reaction. This electrode was named as (SO_x)-NiFeOOH.

In this reaction, Ni foam acts as the source of Ni ions as well as a substrate. The addition of $S_2O_3^{2-}$ to water elevates the pH, which in turn facilitates the redox reaction between Ni foam

and Fe^{3+} results in the formation of Ni^{2+} and Fe^{2+}. These ions combine with OH^- ions and subsequent reaction with thiosulfate ions yields (SO_x)-NiFeOOH on Ni foam.[1]

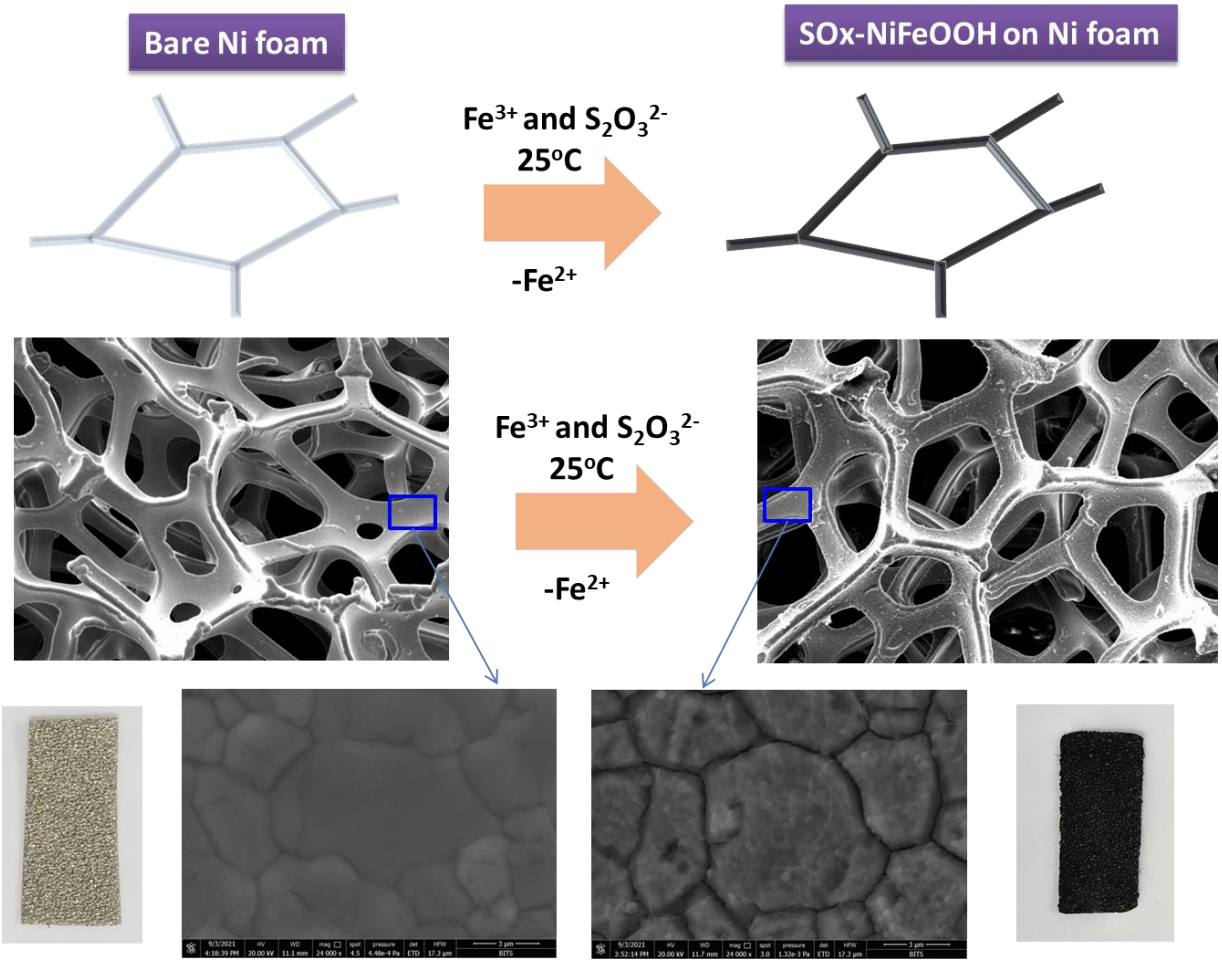

Scheme S1. Schematic depiction of the formation of chalcogenate grafted NiFeOOH on Ni foam. The digital photographs of Ni foam before and after reaction are also shown in the scheme.

Similar protocol has been followed in the absence of $NaS_2O_3.5H_2O$ to prepare films of NiFeOOH on Ni foam. Further, (SO_x) - NiOOH films on Ni foam were obtained using similar procedure, however in the absence of $Fe(NO)_3.9H_2O$.

1.3 Preparation of Ni_2P on Ni foam: Ni_2P was grown on pre-cleaned Ni foam using a modified solvothermal method.[2] Briefly, 3.22 mmol of red phosphorus (Red-P) was added to 20 mL of ethylene diamine, followed by stirring for 30 min. at a speed of 300 rpm at 25 ^oC.

After 30 min, this mixture was transferred to a 50 mL autoclave and a pre-cleaned Ni foam was placed in this mixture. Subsequently, the autoclave was kept in hot-air oven at 160 ^{o}C for 12 h. After 12 h, the autoclave was allowed to cool down to 25 ^{o}C. Subsequently, the Ni foam was removed from the reaction mixture, washed with ethanol, and kept for drying at ambient temperature. A clear dark layer formed on Ni foam indicate the formation of phosphide-based layer on the surface of Ni foam.

1.4 Characterization: Powder XRD patterns were obtained using X-ray diffractometer (Bruker D8 Advance) in the 2θ range of 5 to 90^{o} at a scan rate 3.5 ^{o}/min with Cu-Kα radiation (λ = 1.5405 Å). Morphology of the as-prepared samples was examined using field emission-scanning electron microscope (Quanta FEG250, FEI) (FE-SEM) equipped with energy dispersive X-ray (EDX) analysis. X-ray photoelectron spectroscopy (XPS) measurements were carried out using K-alpha, Thermo Fischer instrument with an Al Kα X-ray source (1486.6 eV). Raman spectra were obtained using LabRAM, Horiba Jobin Yvon Raman microscope with an excitation wavelength of 532 nm. Fourier transform infrared spectroscopy (FTIR) measurements were performed using Perkin Elmer spectrophotometer (Model: spectrum two) in ATR mode. Transmission electron microscopy (TEM), high resolution TEM (HRTEM) and scanning TEM (STEM) were acquired using TALOS F200S G2. Samples for TEM analysis were prepared by drop casting the ethanolic dispersions obtained by sonicating the films on Ni foam, onto carbon coated copper grids and dried under ambient conditions. Ion chromatography (IC) measurements were performed using Metrohm Eco IC. The column used was Metrosep A SUPP 5 -250 and the detector used was UV-vis detector. The eluent used was 10 g/L NaCl. The injection volume of the was 20 µL and flow rate was maintained at 0.7 mL/min

1.5 Electrochemical studies: As-obtained films on Ni foam were studied for their electrochemical properties. Electrochemical tests were performed using an electrochemical

workstation procured from Ivium technologies (Iviumstat). Preliminary electrochemical measurements were carried out in three-electrode setup, wherein, the as-prepared materials on Ni foam acted as working electrodes, graphite rod and Hg/HgO (1 M KOH) (MMO) were the auxiliary and reference electrodes, respectively. Polarization curves were recorded in 1 M KOH for oxygen evolution reaction (OER) and 1 M KOH with known concentration of KI for iodide oxidation reaction (IOR) at a scan rate of 5 mV/s. The pH of the electrolyte was measured to be pH = 13.78. The measured potential vs. MMO was converted into reversible hydrogen electrode (RHE) using the following equation.

$$E_{RHE} = E_{MMO} + E^{o}_{MMO} + 0.059 \times pH \qquad (1)$$

where E^{o}_{MMO} is standard potential of MMO (0.098 V vs. NHE).[1]

Reverse scans were recorded and represented for OER to unambiguously identify the onset potential which eliminates the influence of Ni (II) to Ni (III) faradaic process.

Hydrogen evolution reaction (HER) studies were carried out in 1 M KOH using Ni_2P grown on Ni as working electrode, MMO as reference electrode and graphite rod as auxiliary electrode. The scan rate used was 5 mV/s.

The electrochemical active surface area (ECSA) of all the electrodes were assessed by measuring double layer capacitance (C_{dl}).[1,3] To obtain the C_{dl} of electrocatalysts, cyclic voltammograms were recorded in the non-faradaic region (0.1-0.2 V vs. MMO) at varying scan rates from 20-100 mV/s. The C_{dl} values of all the catalysts were determined from the slope of the plots of $\Delta J/2$ [difference in the capacitive currents ($J_{anodic} - J_{cathodic}$)/2] vs. scanrate. Further, ECSA is calculated according to the following equation.

$$ECSA = \frac{C_{dl}}{C_s} \qquad (2)$$

where C_s is specific capacitance of an ideally flat metallic electrode whose value is 40 μF/cm^2, taken from the literature.[4]

Tafel equation (equation 3) was used to obtain tafel slopes from the polarization data.

$$\eta = a + b \log|j| \quad (3)$$

where b is tafel slope (mV/dec) and j is current density (mA/cm^2). The slope of the plot of potential vs. log j gives tafel slope.

Electrochemical impedance spectroscopic (EIS) measurements were performed at 1.5 V vs. RHE of respective electrodes in a frequency ranging from 10 kHz to 0.1 Hz at an amplitude of 5 mV.

All polarization curves were iR-corrected (100 %) (equation 4) unless otherwise stated.

$$E_{iR\ corrected} = E_{measured} - i \times R_s \quad (4)$$

$E_{measured}$ is the experimentally measured potential, and R_s is the solution resistance obtained from EIS measurements.

The two-electrode electrochemical measurements were carried out using custom-build two compartment H-cell setup in which Ni_2P acted as the cathode for HER and (SO_x)-NiFeOOH served as anode for IOR separated with Nafion™ 211 proton exchange membrane. The capacity of each compartment in the H-cell is 50 mL. The anode compartment contains 30 mL of 1 M KOH and 0.33 M KI while the cathode compartment was filled with 1 M KOH.

Faradaic efficiency (%FE) was calculated using the following formula,

$$\%\ FE = \frac{n \times mole\ of\ H_2\ produced \times F}{Total\ charge\ passed} * 100\ \% \quad (5)$$

where n is the number of transferred electrons, F is the Faraday constant (96,485 C mol^{-1})

Energy-saving efficiency was calculated by the following formula [5]

$$\eta = \frac{(Cell\ voltage\ of\ OER - Cell\ voltage\ of\ IOR)}{(Cell\ voltage\ of\ OER)} \times 100\ \% \qquad (6)$$

Electricity consumption (W) efficiency (kW h N m^{-3}) was calculated using the following formula [6]

$$W = \frac{nFU \times 1000}{3600 \times V_m} \qquad (7)$$

where n is the number of electrons transferred for H_2 generation, F is Faraday's constant, U is the applied voltage, V_m is the molar volume of gas (24.2 L/mol) at 25 ºC

Pseudo-overpotential[7] is calculated as follows,

$$\eta_p = \mathrm{E(IOR@10\ mA}\ cm^2) - E_{eq}\ \mathrm{(OER)} \qquad (8)$$

where, η_p is the pseudo overpotential, E (IOR@10 mA cm^{-2}) is the IOR potential vs. RHE to reach 10 mA cm^{-2} and E_{eq} is the standard thermodynamic potential for OER.[7]

1.6 Gas Quantification:

The evolved gases in traditional (OER//HER) and hybrid electrolysis (IOR//HER) systems were quantified using the water-gas displacement method using a home-built setup. The cathode compartment was filled with 1 M KOH and anode compartment was filled with 0.33 M KI in 1 M KOH. The initial volume in each of these compartments were noted. A cell voltage of 1.7 V was applied and the volume change during electrolysis was monitored.

Studies were also carried out to further validate the determining role of IOR process in boosting H_2 evolution by quantifying H_2 produced in hybrid electrolysis systems at low cell voltages *viz*. 1.3 V. The evolved H_2 gas during these measurements was quantified using gas chromatograph (GC 8890, Agilent) equipped with a molsieve 5A 80/100 SS packed column and a thermal conductivity detector (TCD). Argon gas was used as carrier gas (0.5 mL/min).

Column temperature was maintained at 40 ^{o}C. Injections of 0.2 mL each were made by collecting gases from the headspace of cathode compartment of the H-cell.

1.7 IOR product Quantification:

The product of IOR, iodate (IO_3^-) was qualitatively determined using Raman spectroscopy of the electrode after long term tests. The quantification of iodate was carried out using Iodometry. Briefly, the product collected after chronoamperometry measurements performed at 1.39 V vs. RHE for 6.5 hours was titrated against standardized $Na_2S_2O_3.5H_2O$. The number of moles of the product determined from iodometric titration was used in % FE calculations.

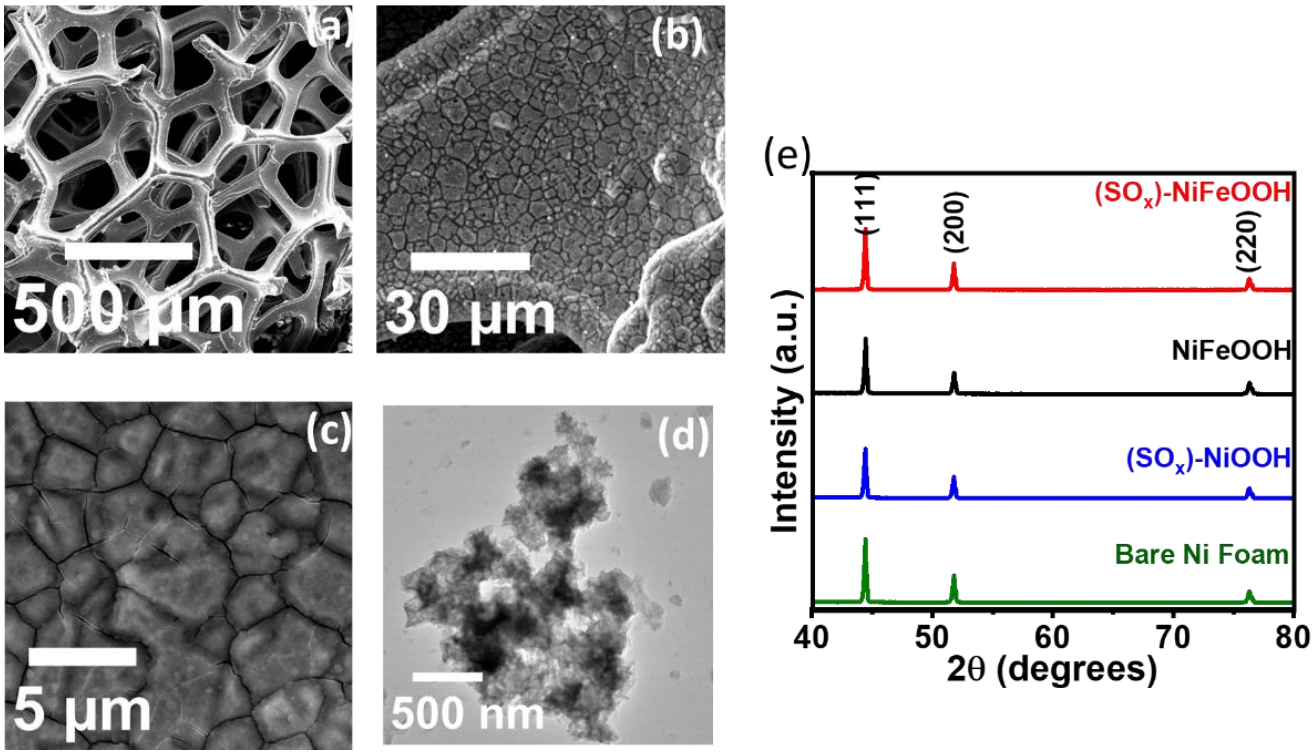

Fig. S1. Fig. S1 (a-c) FESEM images of (SO_x)-NiFeOOH at different magnifications, (d) TEM image of (SO_x)-NiFeOOH, and (e) Powder XRD patterns of (SO_x)-NiFeOOH, NiFeOOH and (SO_x)-NiOOH films prepared on Ni foam along with bare nickel foam.

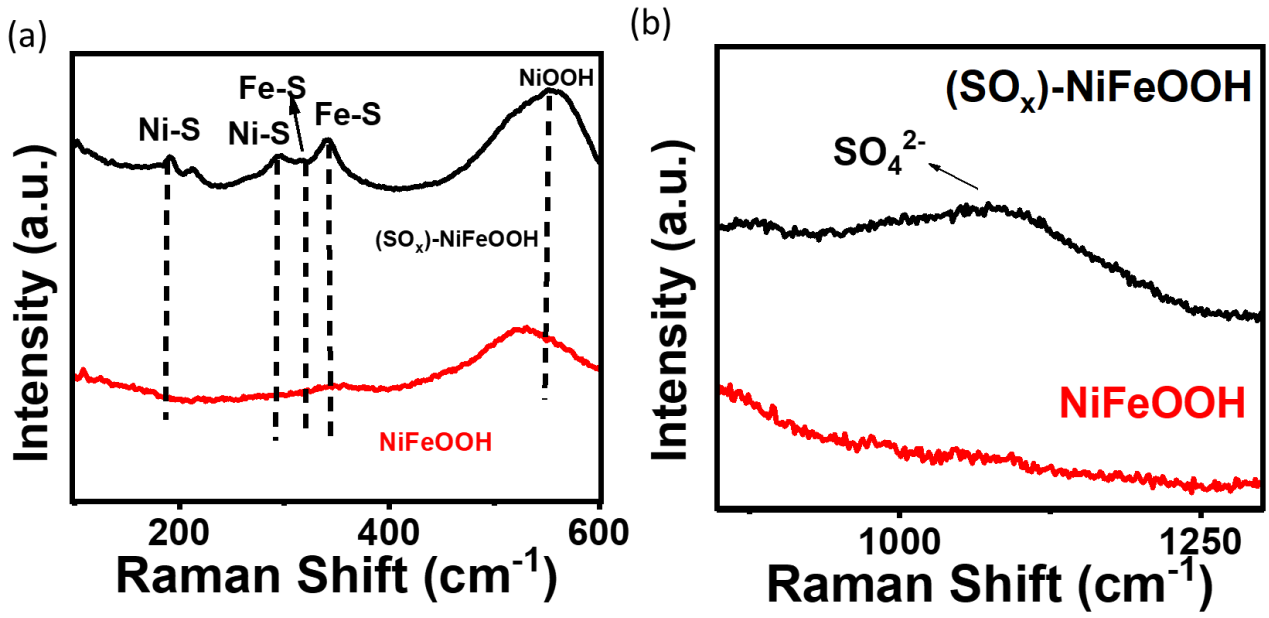

Fig. S2. Raman spectra of (SO_x)-NiFeOOH and NiFeOOH indicate the presence (a) of Ni-S and Fe-S linkages (a), and (b) a broad band corresponding to SO_4^{2-} anchored on the surface of (SO_x)-NiFeOOH.

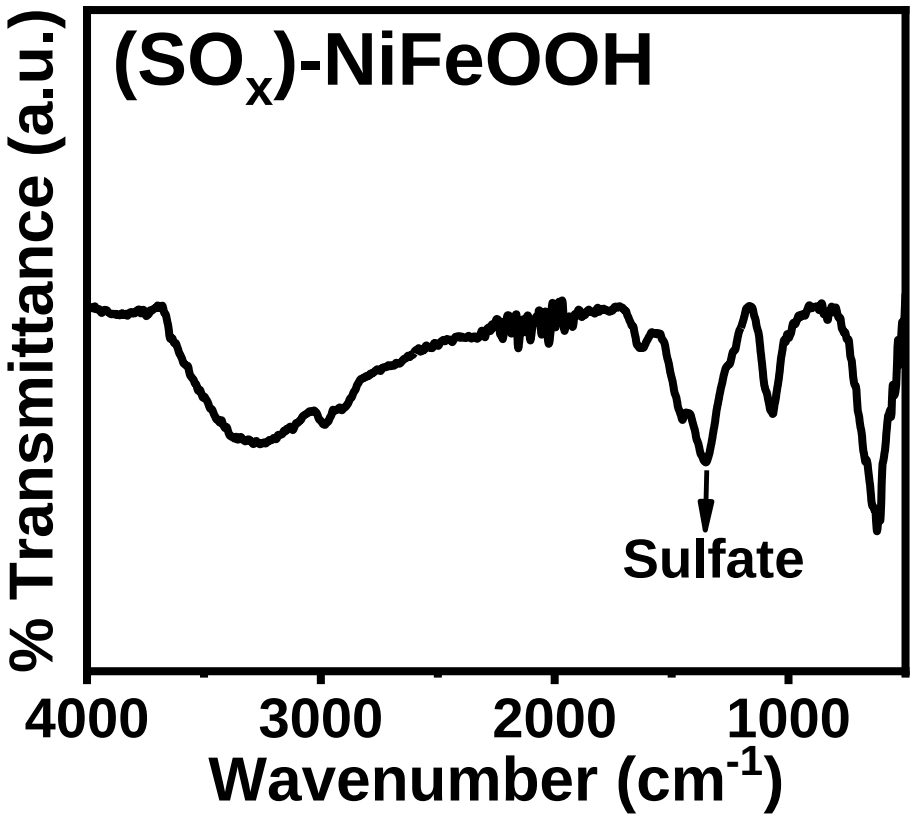

Fig. S3. FTIR spectrum of (SO_x)-NiFeOOH on Ni foam recorded in ATR mode.

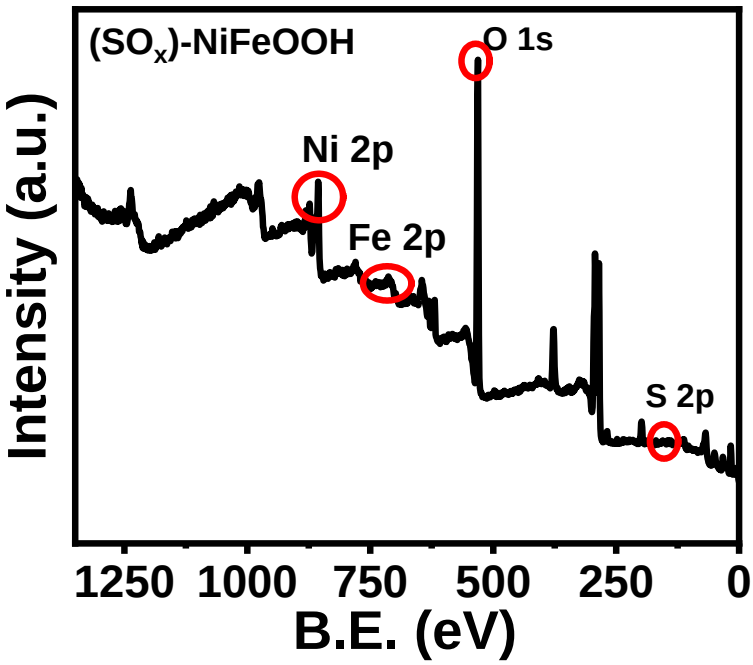

Fig. S4. XPS survey spectrum of (SO_x)-NiFeOOH indicating the presence of Ni, Fe, S and O elements.

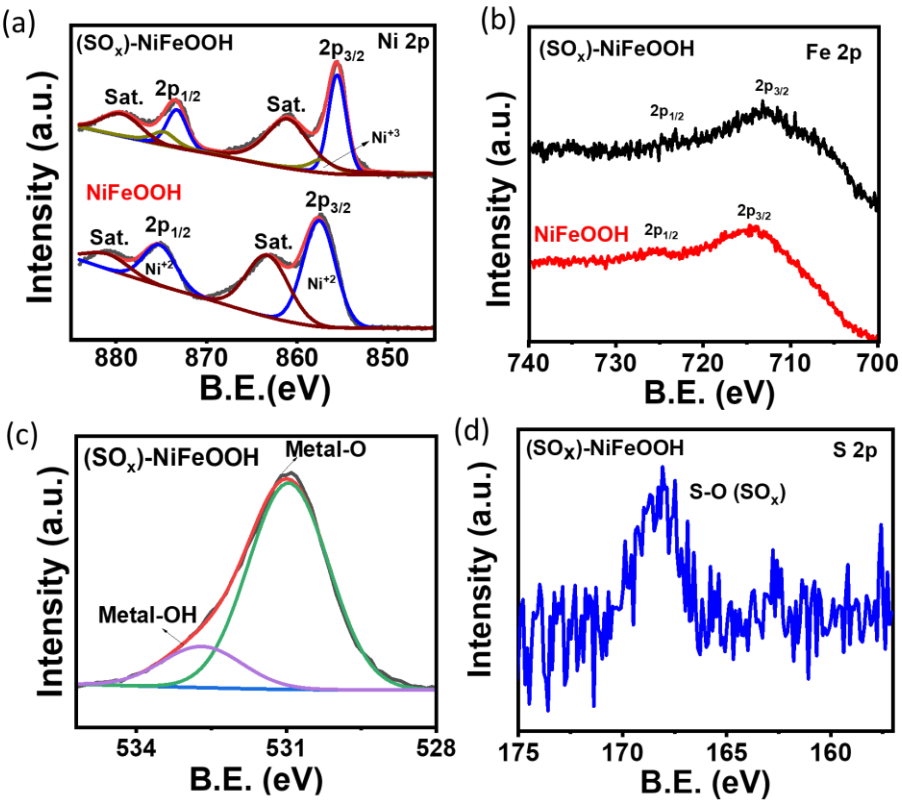

Fig. S5. (a) Ni 2p core-level, (b) Fe 2p core level, (c) S 2p core-level, (d) O 1s core-level XPS spectra of (SO_x)-NiFeOOH. O 1s XPS data indicates the presence of metal-OH and metal-O linkages.

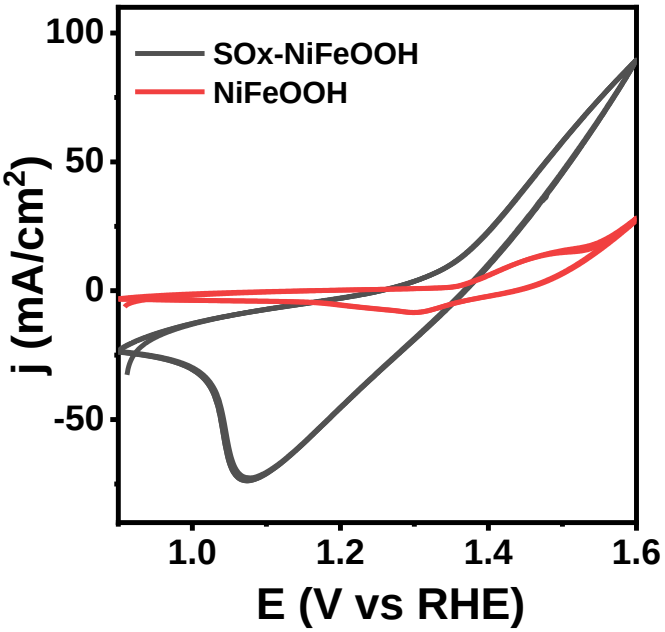

Fig. S6. Cyclic Voltammograms obtained using SO_x-NiFeOOH and NiFeOOH modified Ni foam electrodes in 1 M KOH at a scan rate of 100 mV/s

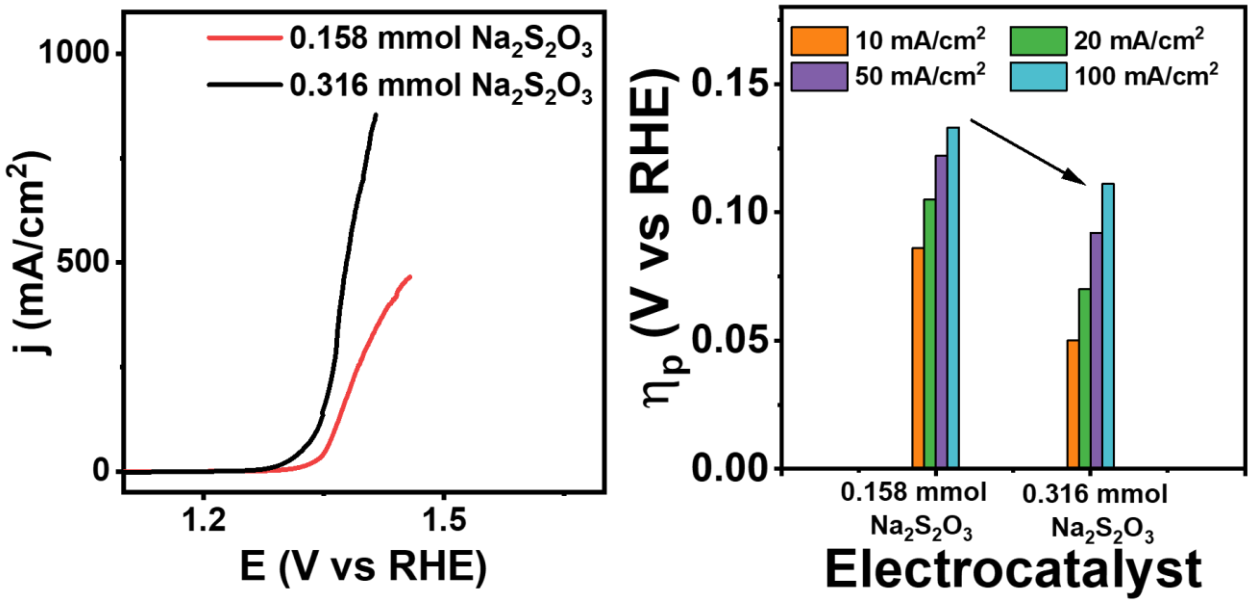

Fig. S7. a. Linear sweep voltammograms obtained using (SO_x)-NiFeOOH films on Ni foam prepared using different amounts of $Na_2S_2O_3.5H_2O$ and b. bar plot depicting the comparison of pseudo overpotential (η_p) at various current densities for IOR.

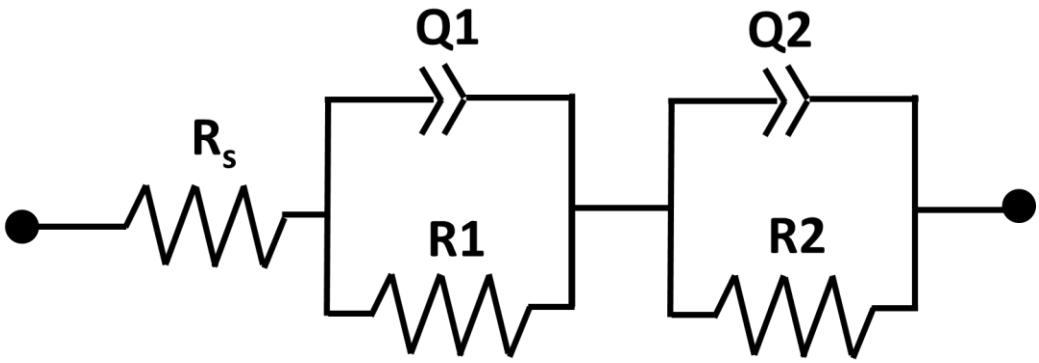

Fig. S8. Equivalent circuit used for fitting the EIS data given in Fig. 3e of the manuscript.

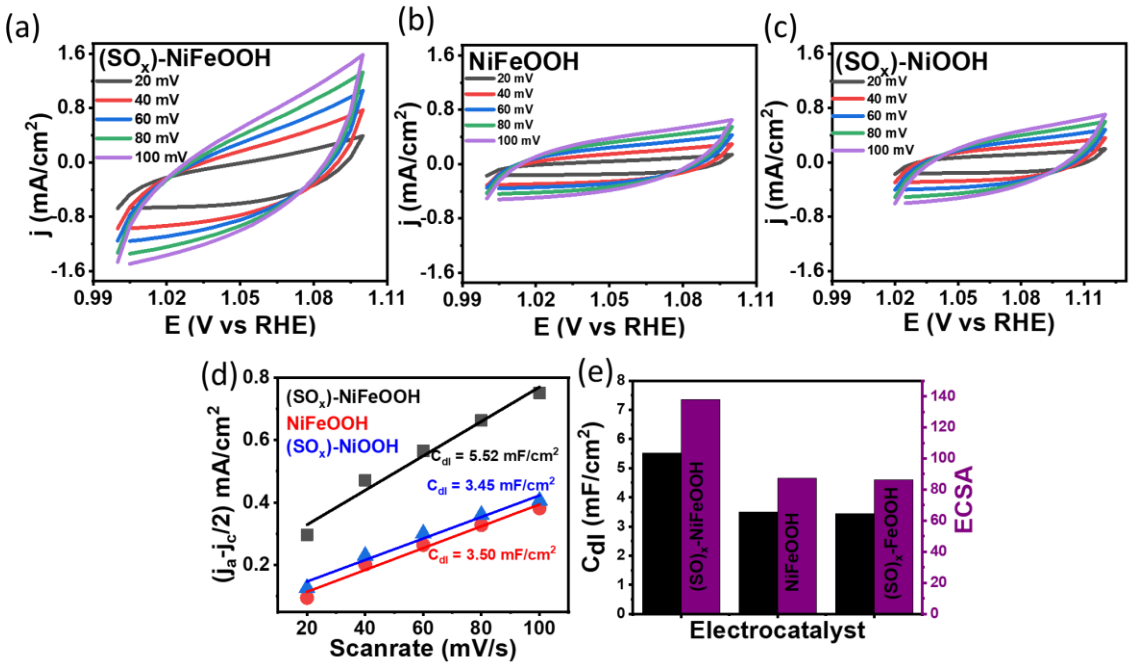

Fig. S9. (a-c) Cyclic voltammograms recorded at different scan rates (20 -100 mV/s) in non-faradaic region using (SO_x)-NiFeOOH, NiFeOOH, (SO_x)-NiOOH in 1 M KOH. (d) Average non-Faradaic current density ($\Delta j = (j_a - j_c)/2$) obtained from CV curves as a function of scan rate, slope gives the electrochemical double layer capacitance (C_{dl}) (e) Plot depicting C_{dl} and electrochemically active surface area (ECSA) of (SO_x)-NiFeOOH, NiFeOOH, (SO_x)-NiOOH. The ranking of ECSA values is (SO_x)-NiFeOOH (138 cm^2) > NiFeOOH (87.5 cm^2) > (SO_x)-NiOOH (86.3 cm^2).

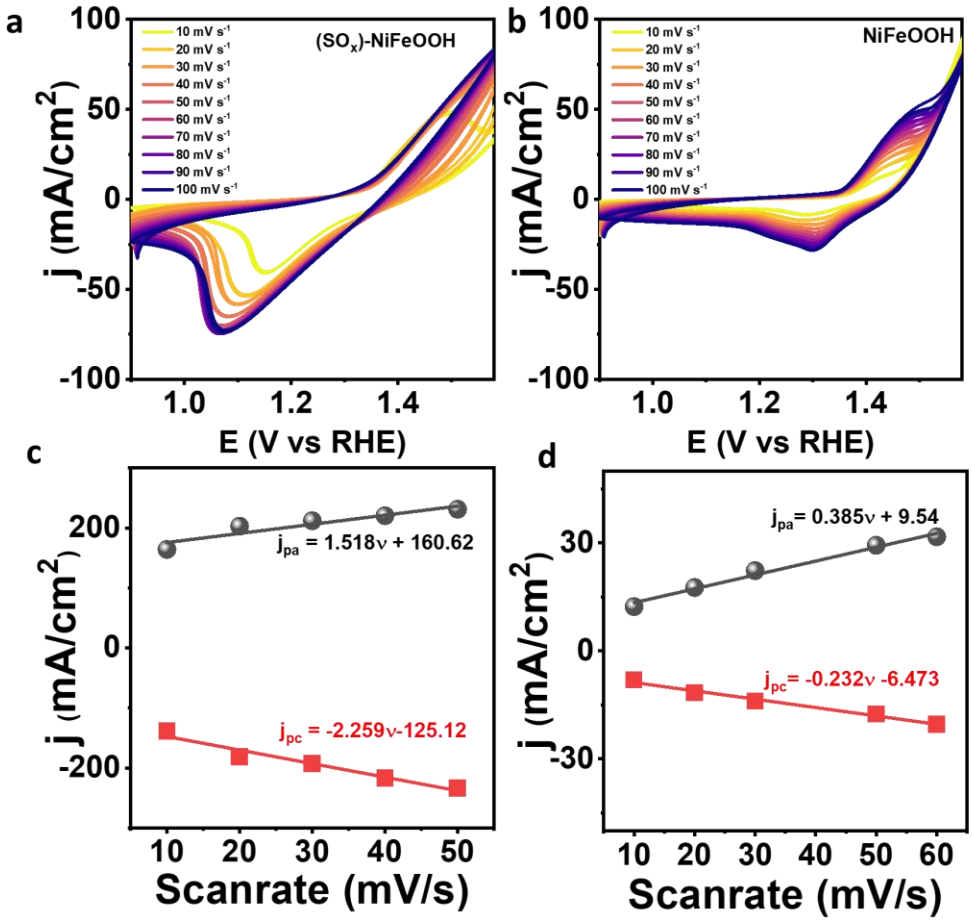

Fig. S10. Cyclic Voltammograms obtained using a. SO_x-NiFeOOH and b. NiFeOOH at different scan rates in the faradaic region for estimating the surface coverage of active species. c & d. Variation of the anodic and cathodic current density with scanrate for SO_x-NiFeOOH and NiFeOOH respectively.

The surface coverage of active species (Γ*) was estimated from the average of anodic and cathodic peak currents vs. scan rate (ν) using the following eqn (8)[8]

$$i_p = (\frac{n^2F^2}{4RT})\Gamma^* A\nu$$

where n, F, R and T are number of electrons transferred (n= 1 in this case), Faraday constant (96845 C mol^{-1}), gas constant (8.314 J K^{-1} mol^{-1}) and temperature respectively. A is the geometric area of the electrode.

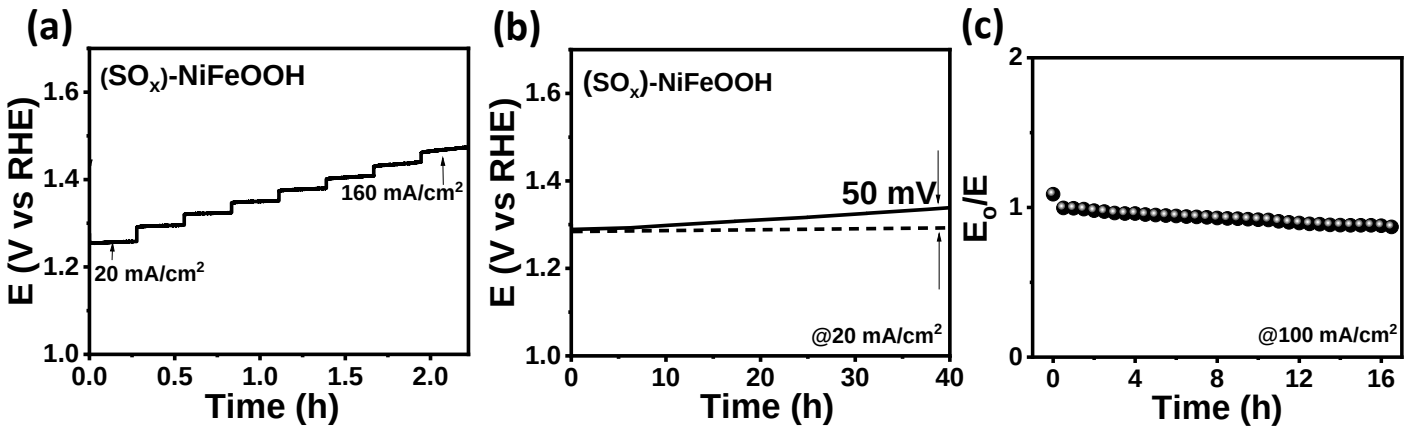

Fig. S11. (a) Multi-step chronoamperometry curve, (b) long-term stability measurement performed at 20 mA cm^{-2}, (c) Variation of normalized potential (E) with respect to potential at t=0 (Eo) as a function of time measured at 100 mA/cm^2 using (SO_x)-NiFeOOH as working electrode in 1 M KOH containing 0.33 M KI.

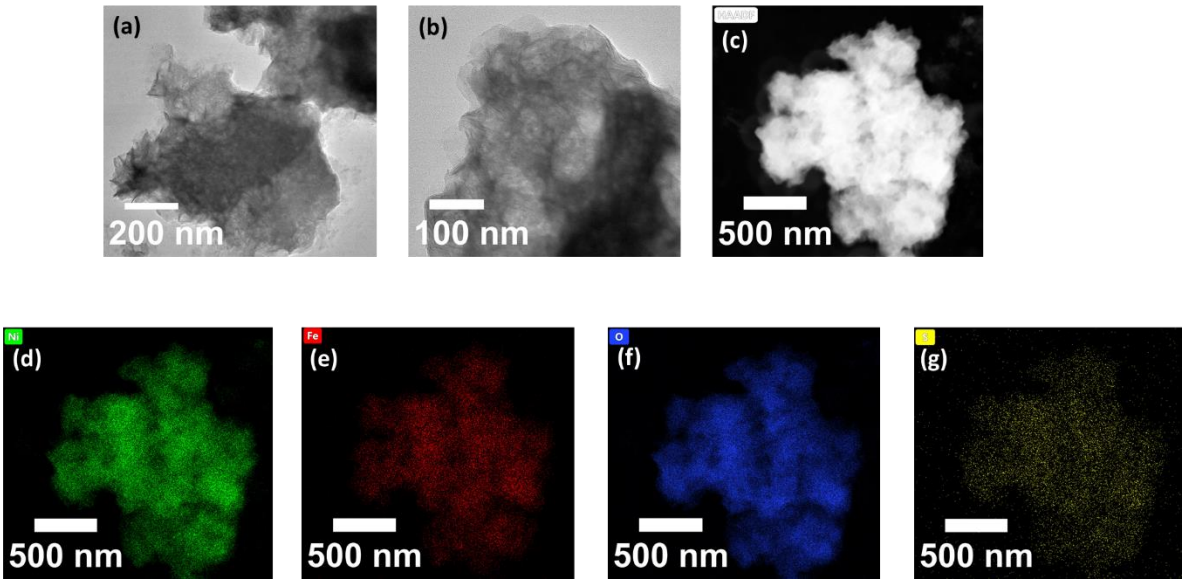

Fig. S12. (a & b) Bright field TEM images, (c) STEM dark field image and (d-g) corresponding elemental mapping images of Ni (d), Fe (e), O (f) and S (g) for the (SO_x)-NiFeOOH after stability tests.

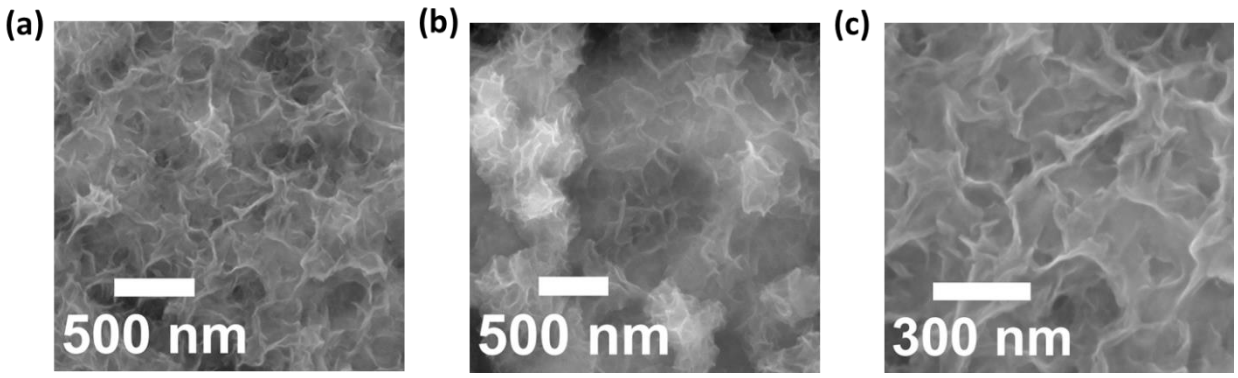

Fig. S13. (a-c) FESEM images of (SO_x)-NiFeOOH recorded after stability tests.

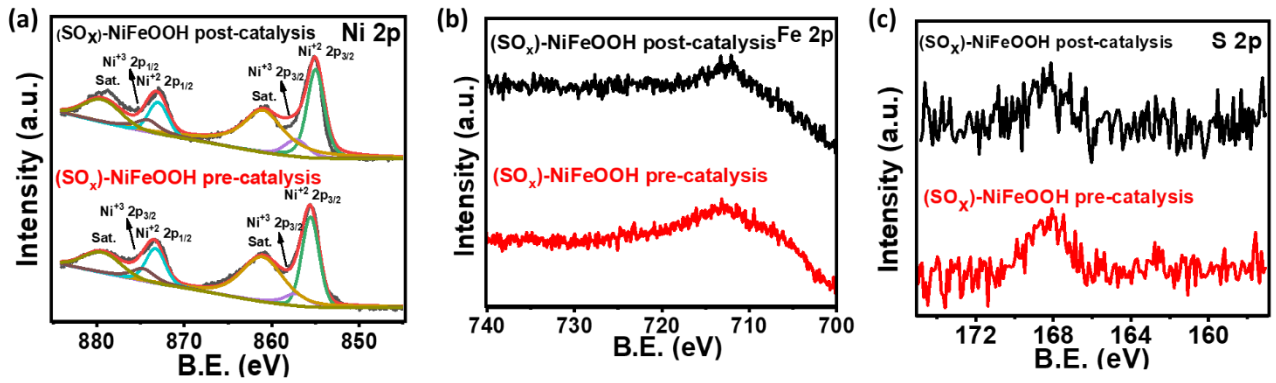

Fig. S14. XPS data of (a) Ni 2p, (b) Fe 2p and (c) S 2p of (SO_x)-NiFeOOH-based electrodes recorded before and after stability tests.

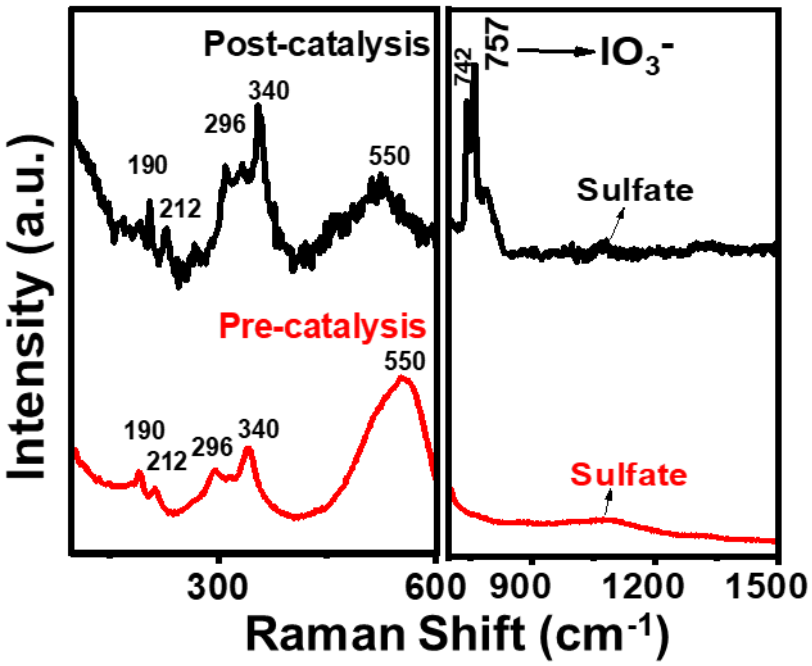

Fig. S15. Raman spectra of (SO_x)-NiFeOOH recorded before and after stability measurements showing characteristics peaks IO_3^- in case of post catalysis sample.

As seen in the Raman spectrum recorded post catalysis for (SO_x)-NiFeOOH, peaks at ~760 cm^{-1} are for Iodate[9] which indicates the formation of IO_3^- as the product of IOR process. Also, the peak for sulfate at ~1025 cm^{-1} is present in the post catalysis sample which further confirms the robustness of the catalyst.[10]

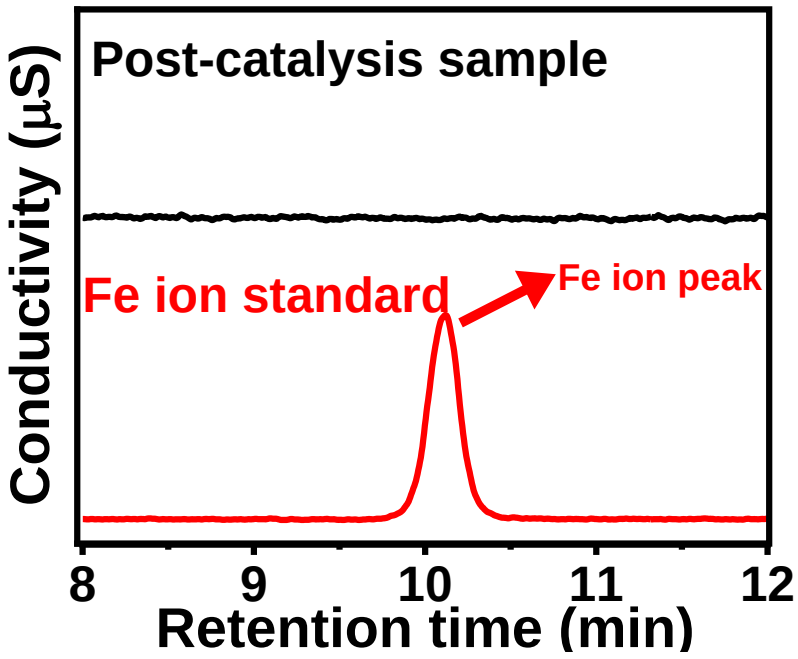

Fig. S16. Ion chromatograms of 5ppm Fe^{+2} standard (red) and the post catalysis sample (black).

As shown in the figure, the ion chromatogram of 5ppm standard solution of Fe^{+2} ions shows a peak at retention time (R_t) 10.2 min. When the post catalysis electrolyte sample was injected, no peak for Fe^{+2} ion was detected in the chromatogram at R_t = 10.2 min, suggesting that the leaching of iron ions from the surface of (SO_x)-NiFeOOH during electrocatalytic measurements is insignificant.

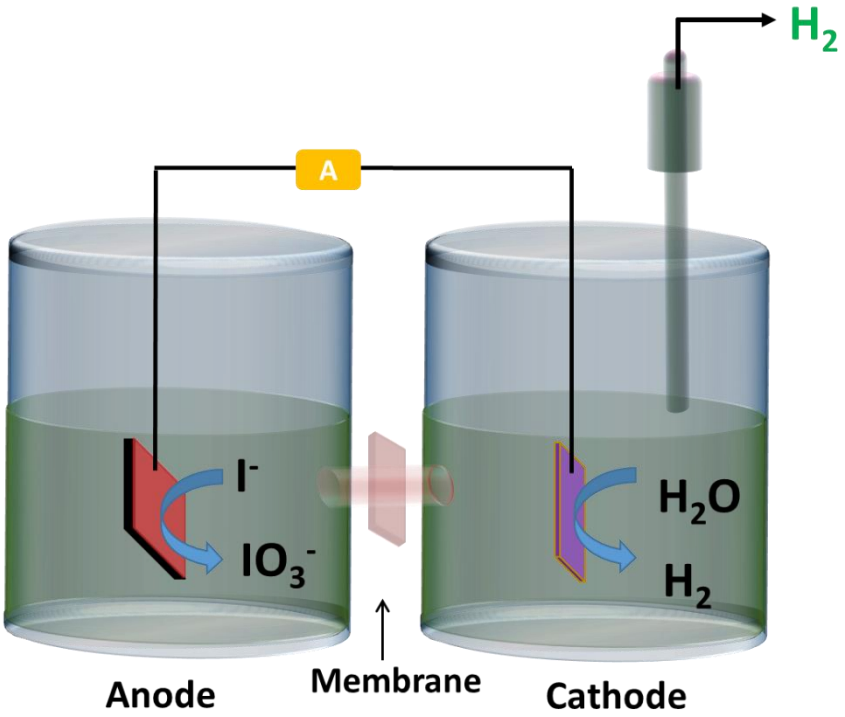

Fig. S17. Schematic representation of two electrode-electrolyser setup for iodide electrolysis (IOR//HER).

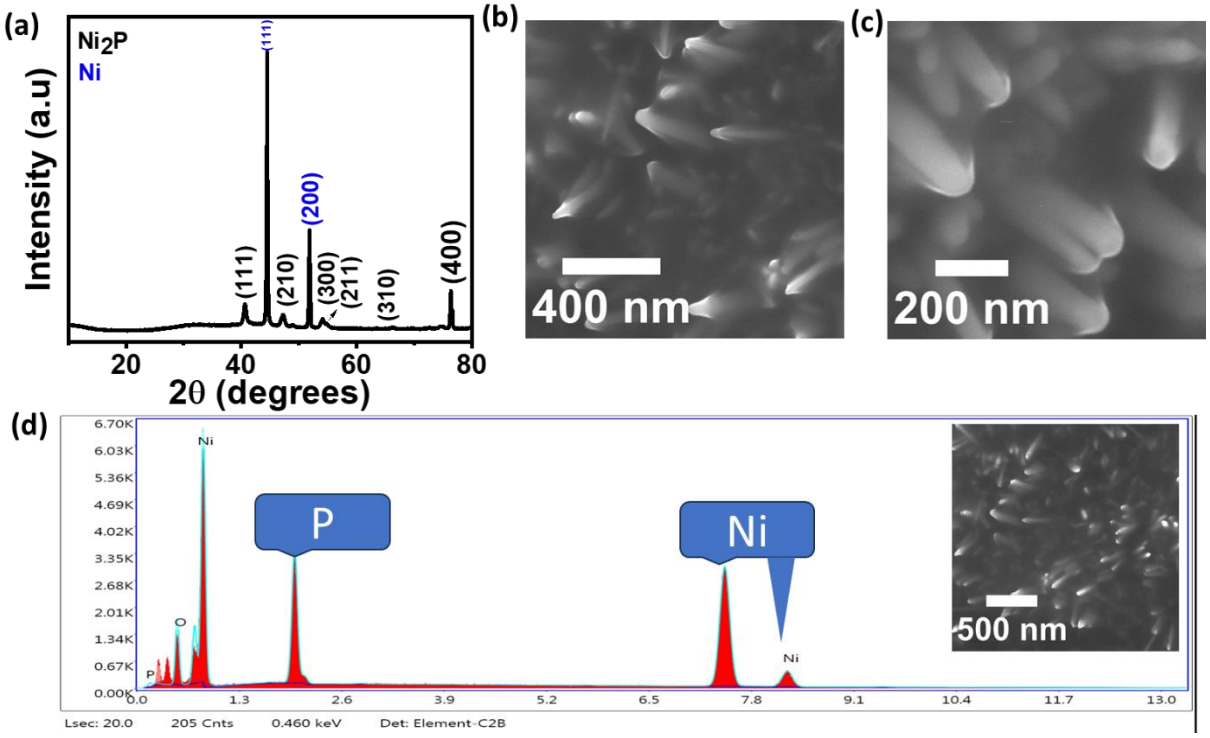

Fig. S18. (a) XRD pattern of Ni_2P nanoneedles grown on Ni foam. (b & c) FESEM images and (d) corresponding EDX spectrum of Ni_2P. Inset of (d) shows the FESEM images of dense Ni_2P nanoneedles.

The XRD data shown in Fig. S18 (a) matches well with Ni_2P phase (ICDD no. 04-003-1863)[2] which indicates the successful formation of Ni_2P on Ni foam. FESEM images shows the nanoneedle morphology of Ni_2P. The EDX spectrum of Ni_2P shows the presence of constituent elements Ni and P.

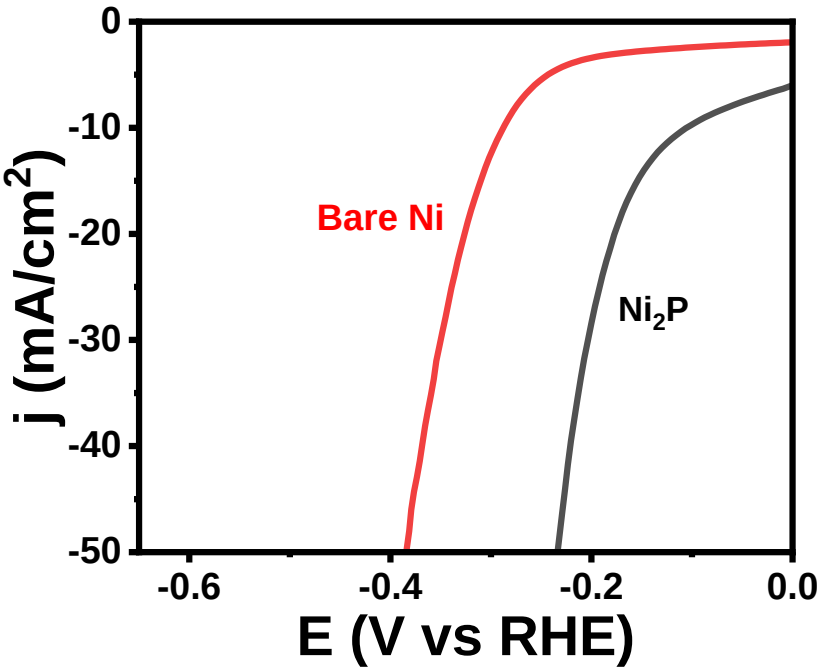

Fig. S19. (a) Linear sweep voltammograms recorded in 1 M KOH at a scan rate of 5 mV/s using Ni_2P (black) and bare Ni foam (red).

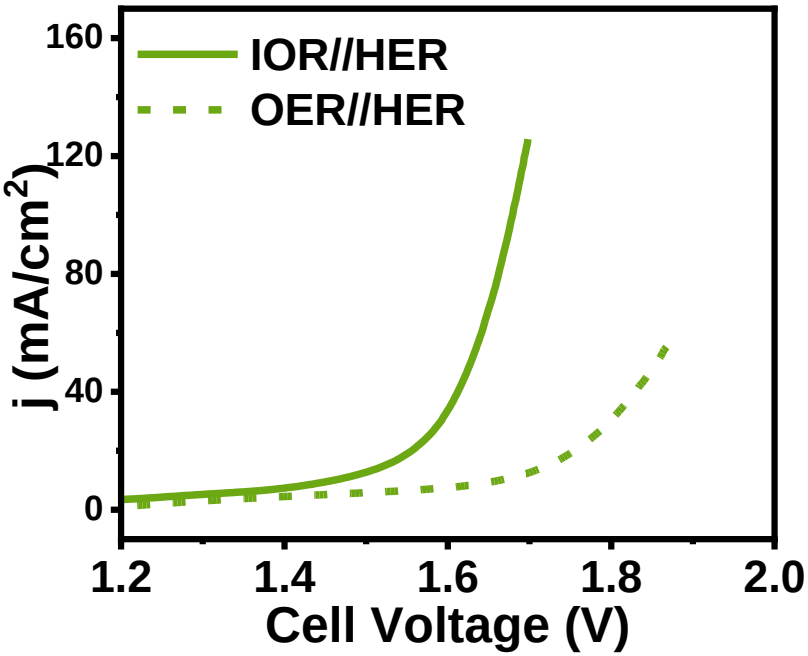

Fig. S20. Polarization data obtained in two electrode-electrolyzer configuration for traditional water electrolysis (dotted line) and iodide electrolysis system (solid line). Pristine NiFeOOH and Ni_2P were used as anode and cathode respectively. Scan rate used was 5 mV/s

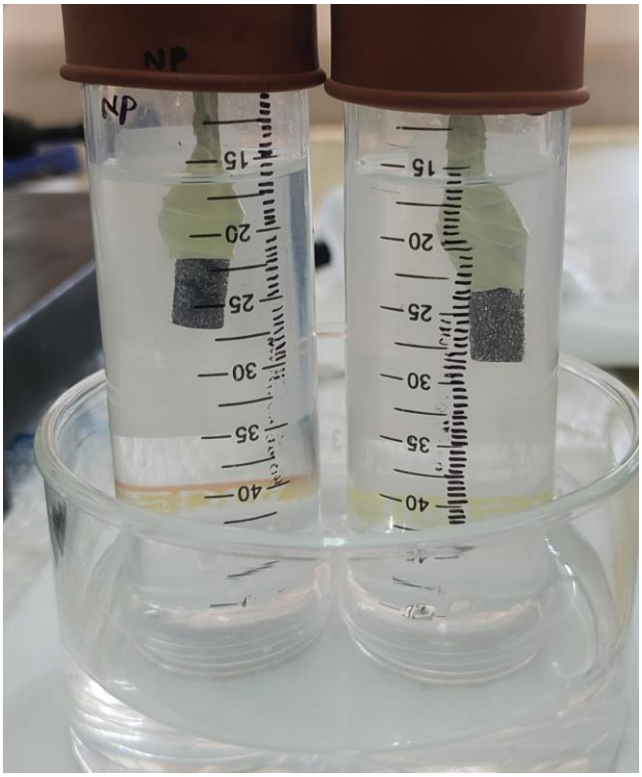

Fig. S21. (a) Digital picture depicting home-built water displacement setup for gas quantification.

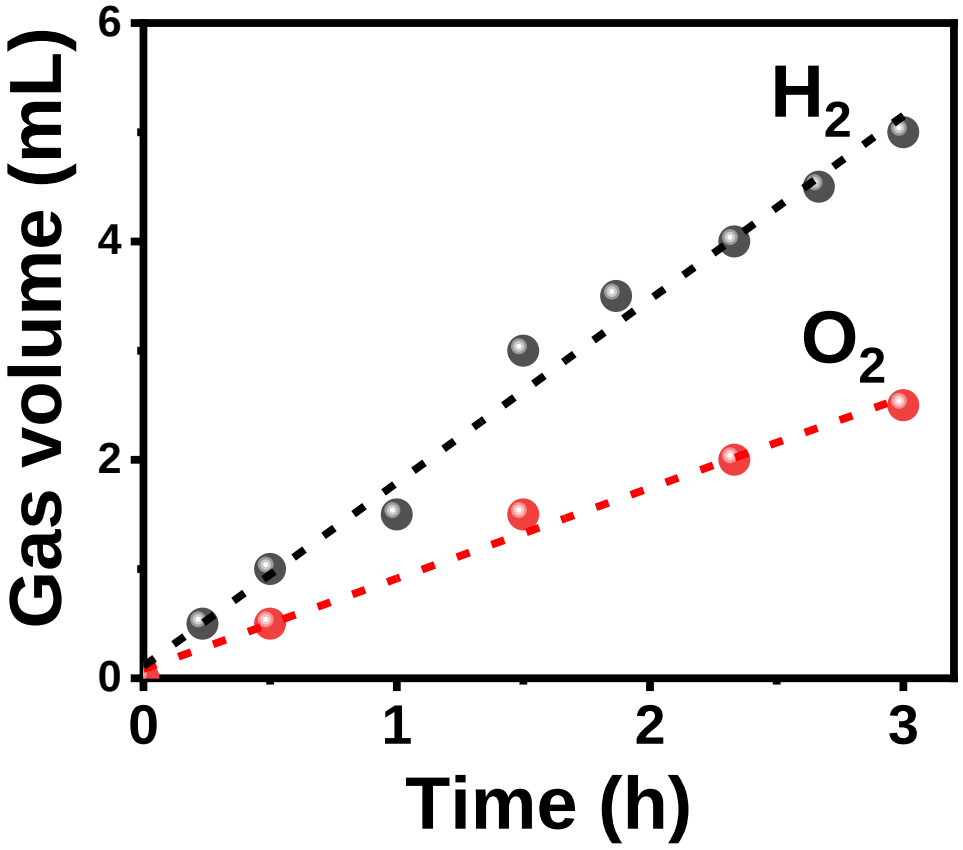

Fig. S22. The gas evolution monitored at cell voltage of 1.7 V as a function of time in a traditional water electrolysis system (IOR//OER) composed of (SO_x)-NiFeOOH as anode and Ni_2P as cathode in 1 M KOH.

A stoichiometric amount (2:1) of H_2 and O_2 are evolved as expected.

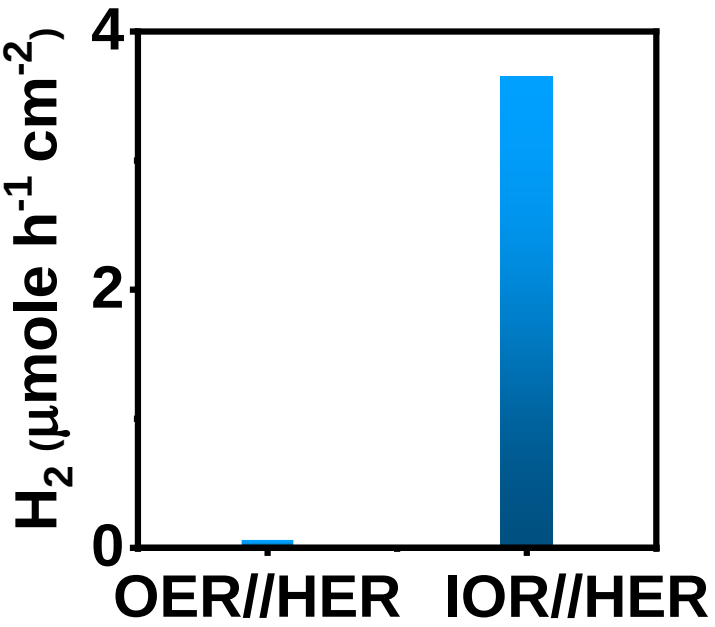

Fig S23. Rate of hydrogen evolution measured at a cell voltage of 1.3 V in traditional (OER//HER) and hybrid (IOR//HER) water electrolysis systems.

Table S1 (Comparison table of various electrocatalysts reported for small molecule oxidation reaction as non-OER process)

S. No.	Catalyst	Electrolyte	Molecule	V (vs RHE) @10 mA/cm^2	V (vs RHE) @100 mA/cm^2	Reference
1	Ni_2P-UNMs/NF	1M KOH	0.125 M Benzylamine	1.34	---	10.1016/j.apcatb.2019.118393
3	$Ni(OH)_2$@NF	1M KOH	0.33M Urea	---	1.44	10.1021/acsaem.0c00122
4	$Ni_2Fe(CN)_6$	1M KOH	0.33M Urea	---	1.35	10.1038/s41560-021-00899-2
5	RhNiFe-P/NF	1 M KOH	0.3 M EtOH	1.37	---	10.1021/acsanm.1c04547
6	Co(II)-CuV	1 M KOH	0.2 M Glycerol	1.39	---	10.1039/D2NA00724J
7	Ni_3N-$Ni_{0.2}Mo_{0.8}N$ NWs/CC	1 M KOH	0.1 M Glycerol	1.30	---	10.1016/j.jechem.2022.04.040
8	Mn-Ni_2P/NiFe LDH	1 M KOH	0.5 M Urea	1.372	1.416 @50 mA/cm^2	10.1039/D3CC01493B
9	Ni-$Co(OH)_2$ NSAs	1 M KOH	0.33 M KI	1.30	---	10.1039/D0NA00847H
10	RuTiO-550	0.1 M NaOH	0.1 M NaI	1.29	---	10.1021/acssuschemeng.1c01867
11	**(SO_x)-NiFeOOH**	**1 M KOH**	**0.33 M KI**	**1.28**	**1.34 V**	**Present Study**

Table S2. Comparison table of various electrocatalysts in two electrode-electrolyzer configuration for small molecule oxidation reaction as non-OER process.

S.No.	Electrocatalyst	Electrolyte	Molecule	V @10 mA/cm^2	Reference
1	VP-Ni(OH)$_2$//CoS$_2$-MoS$_2$	1 M KOH	10 mmol propylamine	1.48	10.1002/anie.202005574
2	Ni$_2$P-UNMs/NF// Ni$_2$P-UNMs/NF	1 M KOH	0.125 M Benzylamine	1.41	10.1016/j.apcatb.2019.118393
3	MoO$_2$-FeP@C// MoO$_2$-FeP@C	1 M KOH	10 mM HMF	1.486	10.1002/adma.202000455
4	Ni-Co(OH)$_2$ NSAs//Ni-Mo	1 M KOH	0.33 M KI	1.34	10.1039/D0NA00847H
5	Mn-Ni$_2$P//NiFe LDH	1 M KOH	0.5 M Urea	1.632	10.1039/D3CC01493B
6	N-CoO$_x$//N-CoO$_x$	1 M KOH	0.1 M Glycerol	1.59	10.1039/D1TA02654B
7	CoOOH//Pt/C	1 M KOH	0.1 M HMF	1.335	10.1039/D0GC04157B
8	Co$_3$S$_4$-NSs/Ni-F//Co$_3$S$_4$-NSs/Ni-F	1 M KOH	1 M EtOH	1.45	10.1021/acsami.0c20554
9	Ni(OH)$_2$/NF// Ni(OH)$_2$/NF	1 M KOH	0.5 M MeOH	1.52	10.1016/j.apcatb.2020.119510
10	**(SO$_x$)-NiFeOOH//Ni$_2$P**	**1 M KOH**	**0.33 M KI**	**1.36**	**Present Study**

References

1. L. Yu, L. Wu, B. McElhenny, S. Song, D. Luo, F. Zhang, Y. Yu, S. Chen and Z. Ren, *Energy Environ. Sci.*, 2020, **13**, 3439-3446.
2. X. Wang, Y. V. Kolen'ko, and L. Liu, *Chem. Commun.,*2015, **51**, 6738-6741.

3. C. C. McCrory, S. Jung, J. C. Peters, and T. F. Jaramillo, *J. Am. Chem. Soc.*, 2013, **135**, 16977-16987.

4. H. Liang, A. N. Gandi, C. Xia, M. N. Hedhili, D. H. Anjum, U. Schwingenschlögl, and H. N. Alshareef, *ACS Energy Lett.,* 2017, **2**, 1035-1042.

5. L. Zeng, W. Chen, Q. Zhang, S. Xu, W. Zhang, F. Lv, Q. Huang, S. Wang, K. Yin, M. Li, Y. Yang, L. Gu, and S. Guo, *ACS Catal.*, 2022, **12**, 11391−11401.

6. T. Wang, Z. Huang, T. Liu, L. Tao, J. Tian, K. Gu, X. Wei, P. Zhou, L. Gan, S. Du, Y. Zou, R. Chen, Y. Li, X. –Z. Fu, and S. Wang, *Angew. Chem., Int. Ed.,* 2022, **61**, e202115636.

7. D. B. Adam, M.-C. Tsai, Y. A. Awoke, W.-H. Huang, C.-H. Lin, T. Alamirew, A. A. Ayele, Y.-W. Yang, C.-W. Pao, W.-N. Su and B. J. Hwang, *Appl Catal., B*, 2022, **316**, 121608.

8. J. Li, L. Li, X. Ma, X. Han, C. Xing, X. Qi, R. He, J. Arbiol, H. Pan, J. Zhao, J. Deng, Y. Zhang, Y. Yang and A. Cabot, *Adv. Sci.,* 2023, **10**, 2300841.

9. M. R. Cicconi, E. Pili, L. Grousset, P. Florian, J. C. Bouillard, D. Vantelon and D. R. Neuville, *Sci. Rep.*, 2019, **9**, 7758.

10. Q. Wen, Y. Lin, Y. Yang, R. Gao, N. Ouyang, D. Ding, Y. Liu and T. Zhai*, ACS Nano*, 2022, **16**, 9572-9582.